

Manipulating Plasma Excitations with Terahertz Light Pulses in Superconducting Cuprates

Jacopo Fiore,^{1,*} Niccolò Sellati,¹ Francesco Gabriele,¹ Claudio Castellani,¹ Goetz Seibold,² Mattia Udina,¹ and Lara Benfatto^{1,†}

¹*Department of Physics and ISC-CNR, "Sapienza" University of Rome, P.le A. Moro 5, 00185 Rome, Italy*

²*Institut für Physik, BTU Cottbus-Senftenberg, PBox 101344, 03013 Cottbus, Germany*

(Dated: October 26, 2023)

Layered cuprates offer a preferential playground for optical non-linearity thanks to the emergence, below T_c , of soft out-of-plane Josephson plasmons. The hallmark of such a non-linearity is the observation of Third Harmonic Generation, that has been theoretically understood as a sum-frequency process involving a two-plasmon excitation. However, recent experiments in cuprates with two planes per unit cell challenge this interpretation, due to the lack of resonant response at the temperature where the driving frequency matches the plasma energy scale, as observed instead in single-layer cuprates. Here we show that such an apparent discrepancy in bilayer systems can be resolved by taking into account the combined effect of light polarization and Josephson-coupling anisotropy on setting the energy range where three-dimensional layered plasma modes can be resonantly excited. Our results offer a novel perspective on the possibility to tune on demand high-harmonic generation by artificially designing Josephson heterostructures.

Introduction. The technical improvements in the generation of intense and phase-stable THz fields[1, 2] considerably enlarged the possibilities to manipulate material properties via optical nonlinearities triggered by ultra-short light pulses. The basic mechanism relies on the possibility of THz radiation to coherently drive large amplitude fluctuations of Raman-active modes, which are quadratically coupled to light. Within this picture, the largest response occurs when *twice* the pump frequency Ω of the THz light matches the mode resonance ω_0 , highlighting the underlying two-photon sum-frequency nature of the excitation process[3–5]. On the other hand, a related but yet different possibility is that strong pulses are able to drive simultaneously two modes, like e.g. infrared-active lattice vibrations[6–10]. In this case, one would expect the response to be larger when the pump frequency matches directly the mode resonance at ω_0 [11, 12]. So far, such a scenario has been mainly discussed within the context of the so-called non-linear phononics[6–10], where the simultaneous excitations of two phonons activates processes mediated by anharmonic coupling between lattice vibrations[13], like e.g. driving silent symmetric modes[14]. However, it has been recently suggested[11] that the same mechanism is also responsible for the non-linear driving of the soft out-of-plane Josephson plasma mode in cuprate superconductors, experimentally observed in systems with both one[15–20] and two layers[21–23] per unit cell.

On general ground, the phase fluctuations of the complex SC order parameter identify the energy scale of plasma modes below T_c [24, 25]. In layered high- T_c cuprates the weak coupling between CuO_2 planes pushes the energy scale of the out-of-plane plasmon in the range of few THz, making it undamped by the opening of the SC gap. This effect usually manifests as a sharp reflectivity plasma edge appearing below T_c at a temperature-

dependent scale $\omega_z(T)$ [26–31]. The optical response of plasma waves is usually linked to effective Josephson-like models[32, 33], that naturally encode a non-linear coupling to light, needed to explain e.g. the Third Harmonic Generation (THG) in the reflected signal[17, 19, 23]. In analogy with non-linear phononics, this effect could then be ascribed[11] to the simultaneous excitations of two plasma waves, leading then to the largest THG at \bar{T} where $\Omega = \omega_z(\bar{T})$. While experiments in single-layer cuprates are consistent with such a picture[17, 19], recent measurements in double-layer YBCO[23] show a monotonic increase of the THG below T_c , without any resonance at the temperature where the pumping frequency matches the value of the plasma edge measured by the out-of-plane reflectivity[27–30, 34].

In this paper we provide a microscopic derivation of the THG response of plasma modes in layered superconductors, showing how the unavoidable entanglement between in-plane and out-of-plane plasma waves, encoded in their momentum dispersion, crucially determines the spectrum of the non-linear optical response. Indeed, since light momentum is essentially zero as compared to lattice momentum, the two plasma waves excited by light have in general two opposite three-dimensional (3D) momenta. Such an effect, neglected in previous work[11], turns out to be crucial to explain the difference between single-layer and bilayer superconductors. The starting observation is that in layered 3D superconductors the dispersive plasmon covers in principle a wide spectrum of energies, see Fig. 1(b), ranging from the soft out-of-plane plasmon ω_z to the large in-plane plasmon ω_{xy} , both identified by reflectivity edges in the the zero-momentum limit. Such a dispersion, that has been recently measured by RIXS experiments in cuprates [35–37], could be expected in principle to wash out any sharp resonance from two-plasmon processes. However, as we show in

the present manuscript, in the single-layer case the light polarization projects out the full plasmon dispersion towards the low-energy ω_z value, making the final response pretty similar to the one computed before[11] by neglecting the plasmon dispersion. For bilayer superconductors the anisotropy of intra-bilayer J_{z1} and inter-bilayer J_{z2} Josephson couplings, with $J_{z1} \gg J_{z2}$, leads to a doubling of the soft plasmons[27–30, 34], with $\omega_{z1} \gg \omega_{z2}$. While the lower one $\omega_{z2}^2 \propto J_{z2}$ controls the lower and sharper reflectivity edge at zero momentum, the dominant contributions of plasma modes to the THG arise from intra-bilayer phase fluctuations, having the larger Josephson stiffness. As a consequence in this case the momentum integration moves the THG spectral weight towards a higher energy scale $\omega_{zT} \approx \omega_{z1}$, explaining the lack of any resonance when the pump frequency matches the value of the lower plasma edge in the measurements of Ref. [23]. Our findings provide a novel perspective on the possibility to tune on demand the non-linear optical response by designing e.g. artificial layered heterostructures with ad-hoc Josephson couplings for non-linear plasmonic applications.

Single layer case. The contribution of plasma waves to the non-linear optical response can be qualitatively understood within a simplified anisotropic Josephson-like model for the phase degrees of freedom. Labelling with θ_n the SC phase in the n -th layer one can write an effective classical Hamiltonian:

$$H = \frac{1}{8} \int d^2r d \sum_n [D_{xy}(\nabla_{xy}\theta)^2 - 8J_z \cos(\theta_{n+1} - \theta_n)], \quad (1)$$

where the in-plane phase difference has been already promoted to a continuum phase gradient, D_{xy} is the in-plane stiffness (equivalent to $\hbar^2 n_s/m$ in the continuum, isotropic limit) and J_z is an energy density defining the superfluid stiffness as $D_z = 4J_z d^2$ along the out-of-plane z direction, d being the interlayer distance. Henceforth, unless explicitly displayed, we set $\hbar = k_B = 1$. The classical model (1) is promoted to a quantum equivalent by including dynamical effects related to the phase gradient in time, scaling as $\kappa_0(\partial_\tau\theta_n)^2$, with κ_0 the charge compressibility. Once that Coulomb effects are included, κ_0 is replaced by the RPA charge compressibility[38, 39]. By retaining only quadratic term in the cosine term of Eq. (1) we obtain the following Gaussian quantum action[40]:

$$S_G = \frac{1}{32\pi e^2} \sum_{i\omega_m, \mathbf{k}} |\mathbf{k}|^2 (-i\omega_m)^2 + \omega_L^2(\mathbf{k}) |\theta(i\omega_m, \mathbf{k})|^2, \quad (2)$$

where $i\omega_m = 2\pi mT$ are bosonic Matsubara frequencies, and ω_L includes the full momentum dependence of the layered Josephson plasma mode (JPM):

$$\omega_L^2(\mathbf{k}) = \omega_{xy}^2 \frac{k_{xy}^2}{|\mathbf{k}|^2} + \omega_z^2 \frac{q_z^2}{|\mathbf{k}|^2}, \quad (3)$$

where $\omega_{xy,z}^2 = 4\pi e^2 D_{xy,z}$, $q_z = (2/d) \sin(k_z d/2)$ and $|\mathbf{k}|^2 = k_{xy}^2 + q_z^2$. As it has been recently discussed in Ref.s [41, 42], the dispersion (3) correctly describes the longitudinal plasma modes at momenta larger than a typical scale $k_c \sim \sqrt{\omega_{xy}^2 - \omega_z^2}/c$ set by the plasma anisotropy. Indeed, below k_c in the layered system the longitudinal (plasmon) and transverse (polariton) modes become intrinsically mixed. Their dispersion should then be computed by taking into account also retardation effects, that in the language of the phase-only model (1) stem from the coupling of the SC phase to the internal gauge field. However, as discussed in the Supplementary[40], the mixing region covers a negligible phase-space contribution in the non-linear kernel, making the approximate form (3) quantitatively valid. An external gauge field A_z polarized along the z direction can be coupled to the model (1) via the minimal coupling substitution $\theta_{n+1} - \theta_n \rightarrow \theta_{n+1} - \theta_n - 2edA_z/c$. The third-order current J^{NL} can be obtained by expanding the cosine Josephson interaction in Eq. (1) beyond second order in the gauge-invariant phase gradient along z , and integrating out the phase degrees of freedom[11]. As detailed in the Supplementary[40] $J^{NL} \sim KA_z^3$, such that for a monochromatic incident field $A_z = A_0 \cos(\Omega t)$ the resulting THG intensity is proportional[5, 43] to $I_{THG} \propto |K(2\Omega)|^2$. For the Josephson model of Eq. (1) the resonant part of the non-linear kernel K accounts for the convolution between two JPMs with opposite momenta, and it is given explicitly by:

$$K(\Omega) \propto J_z^2 \frac{1}{V} \sum_{\mathbf{k}} \frac{q_z^4}{|\mathbf{k}|^4 \omega_L(\mathbf{k}) (4\omega_L^2(\mathbf{k}) - (\Omega + i\delta)^2)}, \quad (4)$$

where the analytical continuation $i\omega_m \rightarrow \Omega + i\delta$ has been performed and momenta integration is limited to the range $k_{xy} < 1/\xi$, with ξ the in-plane coherence length, and $k_z < \pi/d$, i.e. in the \mathbf{k} -region where a phase-only model can be defined. Within the Josephson model (1) the coupling J_z controls both the stiffness and the anharmonic interaction terms. Even though it is known that the quantum Josephson model is just an approximation for the microscopically-derived anharmonic phase model[38], as a first step we will rely on such a description and we will adopt the same experimental temperature-dependent stiffness $D_z(T)$, $D_{xy}(T)$ both in the plasmon dispersion (3) and in the effective anharmonic couplings (see [40] for further details). In addition, even though the layered structure couples in principle also the polariton mode to the external gauge field, its contribution to the non-linear response is quantitatively irrelevant due its fast growing energy scale at finite momentum, as detailed in the Supplementary[40].

In Fig. 1 we show the nonlinear kernel K as a function of temperature and frequency, by comparing the case where the full plasmon dispersion (3) is included (panel c) with the case, considered previously[11], where $\omega_L(\mathbf{k})$ is

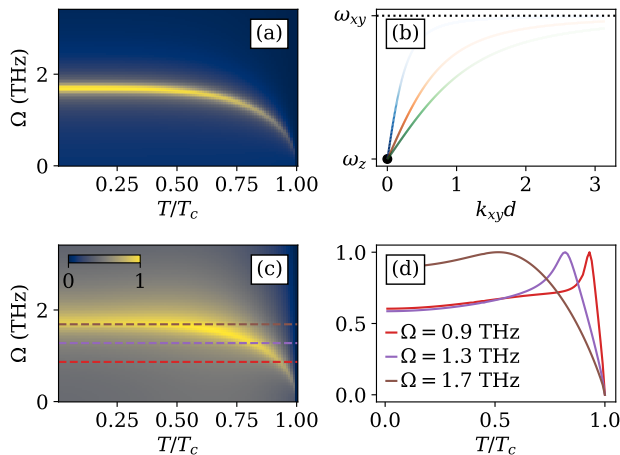


FIG. 1. Comparison between the nonlinear kernel $|K(2\Omega)|$ of Eq. (4) for (a) non-dispersive plasmon, corresponding to replace $\omega_L(\mathbf{k})$ with ω_z , and (c) the dispersive plasmon. (b) Plasmon dispersion $\omega_L(\mathbf{k})$ from Eq. (3) for three selected k_z values as a functions of k_{xy} . The intensity of each line is weighted as $(q_z/|\mathbf{k}|)^4$ to visualize the projector in Eq. (4). (d) $|K(2\Omega)|$ from panel (c) as a function of temperature for three selected pump frequencies (dashed lines in panel (c)), where each curve is normalized to its maximum. Here we set $\omega_{xy}(T=0) = 250$ THz, $\omega_z(T=0) = 1.7$ THz, $\delta = 0.1\omega_z(T=0)$ and $T_c = 38$ K, as appropriate for optimally-doped LSCO samples.

assumed to be non dispersive (panel a). The latter case is equivalent to setting $\omega_L(\mathbf{k}) = \omega_z$ in Eq. (4), which results in a resonance at $\Omega = \omega_z$ of the kernel $K(2\Omega)$. As one can see, even though the dispersive case leads to a smearing of such a sharp resonance, the non-linear kernel shows nonetheless a marked maximum around ω_z , see panel (c). The reason can be easily understood by close inspection of Eq. (4): here the overall factor $q_z^4/|\mathbf{k}|^4$ accounts for the polarization of the light in the z direction, coupling the external e.m. field to a phase gradient between the planes. As a consequence, the full dispersion (3) for the longitudinal plasma mode is projected out on the phase space where $q_z/|\mathbf{k}|$ is dominant, that corresponds to an energy around ω_z . This effect is visualized in Fig. 1b, where the intensity of the line is proportional to the contribution of the mode to the non-linear kernel (4). The enhancement of the kernel at energies around ω_z leads to a non-monotonic T dependence of the THG measured at a fixed pump frequency $\Omega < \omega_z(T=0)$. In Fig. 1d we plot $|K(2\Omega, T)|$ for the three frequencies Ω marked by horizontal lines in panel 1c: even though the exact shape of the THG signal depends on the ratio $\Omega/\omega_z(T=0)$, we nonetheless observe a maximum at the temperature \bar{T} where $\Omega = \omega_z(\bar{T})$, in qualitative agreement with the result obtained for a non-dispersive plasmon[11].

Bilayer case. In the bilayer case one has two planes per unit cell in the z direction, so that the phase variable

$\theta_{\lambda,n}$ has an additional index $\lambda = 1, 2$ denoting the two layers in each unit cells. The out-of-plane hamiltonian density is

$$\mathcal{H}_n^\perp = -J_{z1} \cos(\theta_{1,n} - \theta_{2,n}) - J_{z2} \cos(\theta_{1,n+1} - \theta_{2,n}), \quad (5)$$

in close analogy with Eq. (1), while the in-plane part has the same form. Here we introduced two different Josephson couplings J_{z1} and J_{z2} , with $J_{z1} \gg J_{z2}$, corresponding to a phase difference between the two nearest planes within the same unit cell (at distance $d_1 \sim 3.2$ Å) or in neighboring cells (at distance $d_2 \sim 8.2$ Å), $d = d_1 + d_2$ being the periodicity in the z direction[30, 42, 44], see Fig. 2(a). The corresponding stiffnesses $D_{z\lambda} = 4J_{z\lambda}d_\lambda^2$ are also anisotropic. By introducing the spinor $\bar{\theta} = (\theta_1, \theta_2)$ the generalization of the Gaussian quantum action (2) to the bilayer case reads[40]

$$S_G = \frac{1}{64\pi e^2} \sum_{i\omega_m, \mathbf{k}} \bar{\theta}(-k) \mathcal{K}^2 (-i\omega_m)^2 \mathbb{1} + \Omega_L^2(\mathbf{k}) \bar{\theta}(k). \quad (6)$$

Here we introduced the 2×2 matrix $\mathcal{K}^2 = k_{xy}^2 \mathbb{1} + \mathcal{K}_z^\dagger \mathcal{K}_z$ which generalizes the quadratic term in momentum, where

$$\mathcal{K}_z = \frac{\sqrt{2}}{d} \begin{pmatrix} -\frac{e^{-ik_z d_1/2}}{\sqrt{d_1/d}} & \frac{e^{ik_z d_1/2}}{\sqrt{d_1/d}} \\ \frac{e^{ik_z d_2/2}}{\sqrt{d_2/d}} & -\frac{e^{-ik_z d_2/2}}{\sqrt{d_2/d}} \end{pmatrix}, \quad (7)$$

keeps track of the discretization of the phase variables along the z direction. Analogously $\Omega_L^2(\mathbf{k})$ generalize the plasma dispersion, with $\Omega_L^2(\mathbf{k}) = (\mathcal{K}^2)^{-1}(\omega_{xy}^2 k_{xy}^2 \mathbb{1} + \mathcal{K}_z^\dagger \Omega_z^2 \mathcal{K}_z)$, where $(\Omega_z^2)_{\lambda\mu} = \delta_{\lambda\mu} \omega_{z\lambda}^2$ and $\omega_{z\lambda}^2 = 4\pi e^2 D_{z\lambda}$. From the structure of Eq. (6) one readily sees that the doubling of the layers per unit cell leads to a doubling of the JPMs, defined as the square-root of the eigenvalues of the matrix $\Omega_L^2(\mathbf{k})$, and shown in Fig. 2b. The upper plasmon $\omega_1(\mathbf{k})$, dispersing between ω_{z1} and ω_{xy} , is the equivalent of the single-layer plasmon $\omega_L(\mathbf{k})$, while the additional low-energy out-of-plane plasmon $\omega_2(\mathbf{k})$, dispersing away from ω_{z2} , is characteristic of the bilayer case. As one can see, for increasing in-plane momentum $\omega_2(\mathbf{k})$ evolves rapidly towards an energy scale $\omega_{zT} = \sqrt{(\omega_{z1}^2 d_2 + \omega_{z2}^2 d_1)/d} \approx \omega_{z1}$ for $J_{z1} \gg J_{z2}$, usually named *transverse* plasmon in the literature because it identifies the scale of a resonance peak in the c -axis optical conductivity [27, 34]. For even larger values of k_{xy} $\omega_2(\mathbf{k})$ grows slowly towards the in-plane frequency ω_{xy} . As discussed in Ref. [42], the behavior of the lower plasmon can be intuitively understood as a back-folding at $q_z = 0$ of the $q_z = \pi/d$ soft plasmon of the single-layer, due to the breaking of the periodicity along z when $J_{z1} \neq J_{z2}$.

The computation of the non-linear kernel follows the same steps as before, with both plasmon branches contributing to the out-of-plane response, so that $K(\Omega) =$

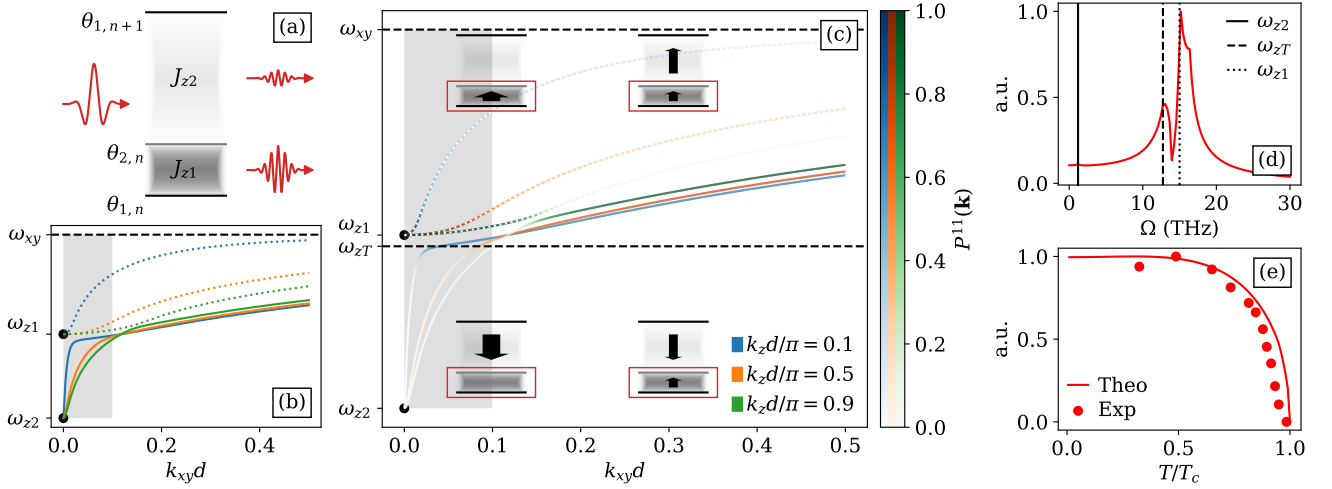


FIG. 2. (a) Sketch of the c -axis non-linear response for the YBCO bilayer system. Since $J_{z1} \gg J_{z2}$ the THG signal is mainly determined by the intra-bilayer phase fluctuations. (b) Plasmon branches $\omega_1(\mathbf{k})$ (dotted lines) and $\omega_2(\mathbf{k})$ (solid lines) at selected k_z for a wide range of k_{xy} value. (c) Zoom-in of panel (c) in the region of interest for the THG, as denoted by the grey shaded area corresponding to the region $k_{xy} < 1/\xi$ of allowed in-plane momenta, where $\xi \sim 10d$ is the in-plane coherence length. Here the line intensity is rescaled according to the relative weight of intra-bilayer phase fluctuations $\tilde{\mathcal{P}}_{\sigma}^{ii}$ of each mode, shown as a color-bar on the right of the panel. A sketch of the corresponding polarizations of the modes[42] in each momenta region is also reported. (d) Frequency dependence of the non-linear kernel $|K(2\Omega)|$ at $T = 0$. Vertical bars denote the position of ω_{z1} , ω_{zT} and ω_{z2} . (e) Temperature dependence of the non-linear kernel $|K(2\Omega)|$ (solid line) for fixed pump frequency $\Omega = 0.5$ THz. The dots represents the experimental data from Ref. [23].

$K_+(\Omega) + K_-(\Omega)$, where

$$K_{\pm}(\Omega) = \sum_{\sigma\sigma', \mathbf{k}} W_{\sigma\sigma'} \frac{\omega_{\sigma} \pm \omega_{\sigma'}}{4\omega_{\sigma}\omega_{\sigma'}} \frac{\coth(\frac{\beta\omega_{\sigma}}{2}) \pm \coth(\frac{\beta\omega_{\sigma'}}{2})}{(\omega_{\sigma} \pm \omega_{\sigma'})^2 - (\Omega + i\delta)^2} \quad (8)$$

combines two JPMS from the same ($\sigma = \sigma'$) or from different ($\sigma \neq \sigma'$) plasmon branches, with $\sigma, \sigma' = 1, 2$, weighted by the \mathbf{k} -dependent projectors $W_{\sigma\sigma'}$. As we already discussed in the single-layer case, the light polarization, encoded here in the $W_{\sigma\sigma'}$ prefactors, projects out the contribution of each mode at selected region of momenta. A full numerical computation of the kernel (8) at low T for parameter values appropriate for YBCO[34] is shown in Fig. 2d. As one can see, $|K(2\Omega)|$ shows two marked resonances near the values $\Omega \approx \omega_{zT} \sim 11$ THz and $\Omega \approx \omega_{z1} \sim 15$ THz, without any signature at the lower plasmon $\omega_{z2} \sim 1.2$ THz, that is the energy scale defining instead the sharp plasma edge in the c -axis reflectivity below T_c [27, 29, 30, 34].

A better insight into this result can be obtained by introducing a new sets of phase variables, corresponding to the intra-bilayer $\tilde{\theta}_1 \sim \theta_{2,n} - \theta_{1,n}$ and inter-bilayer $\tilde{\theta}_2 \sim \theta_{1,n+1} - \theta_{2,n}$ phase gradient in the n -th unit cell, respectively. As manifest from (5), the larger scale J_{z1} couples the gauge field A_z to $\tilde{\theta}_1$, while J_{z2} controls its coupling to $\tilde{\theta}_2$. As detailed in the Supplementary Material[40], by changing basis from (θ_1, θ_2) to $(\tilde{\theta}_1, \tilde{\theta}_2)$ one can write the projectors as $W_{\sigma\sigma'} \propto \text{Tr}(\tilde{\mathcal{P}}_{\sigma}\mathcal{C}\tilde{\mathcal{P}}_{\sigma'}\mathcal{C})$, where the diagonal matrix $(\mathcal{C})_{\lambda\mu} = D_{z\lambda}d_{\lambda}^2\delta_{\lambda\mu}$ comes

from the coupling with the gauge field ($\sim D_{z\lambda}A_z^2d_{\lambda}^2$) and the matrix $\tilde{\mathcal{P}}_{\sigma}$ weights each plasmon branch according to its projection onto inter-bilayer (11 element) and intra-bilayer (22 element) phase fluctuations. Since $D_{z1} \gg D_{z2}$, one immediately recovers that the dominant contribution to the THG of each plasmon branch comes from the phase-space in momenta where they have a large intra-bilayer component, so that one can approximately put $K(\Omega) \sim J_{z1}^2/V \sum_{\mathbf{k}, \sigma} \tilde{\mathcal{P}}_{\sigma}^{11}(\mathbf{k})F(\Omega, \omega_{\sigma}(\mathbf{k}))$, where $F(\Omega, x) = \coth(\beta x/2)/[x(\Omega^2 - 4x^2)]$ and $\tilde{\mathcal{P}}_{\sigma}^{11}(\mathbf{k})$ are the intra-bilayer components of the projector $\tilde{\mathcal{P}}_{\sigma}$.

In Fig. 2c the plasmon dispersions at selected k_z are plotted as a function of k_{xy} using a color-code for the line intensity corresponding to their projection $\tilde{\mathcal{P}}_{\sigma}^{11}(\mathbf{k})$ on the intra-bilayer fluctuations. The upper plasmon branch $\omega_1(\mathbf{k})$ is purely intra-bilayer for zero in-plane momentum, and gradually acquires an inter-bilayer component as k_{xy} increases. Thus, the result of the weighting factor is to select the low-momenta region where $\omega_1(\mathbf{k}) \approx \omega_{z1}$, as already observed for the $\omega_L(\mathbf{k})$ in the single-layer case. Conversely the lower plasmon branch $\omega_2(\mathbf{k})$ has exactly zero intra-bilayer projection at $k_{xy} = 0$, being associated with purely inter-bilayer phase fluctuations[40, 42]. As a consequence it only contributes to the non-linear kernel in the momenta region where it evolves towards the ω_{zT} energy scale, explaining the lack on any signature at ω_{z2} observed in the numerical result of Fig. 2d.

Discussion. The present results for the two-plasmon contribution to the non-linear response account very

well for recent measurements in single-layer and bilayer cuprates. In the single-layer case, where a single out-of-plane plasma mode exists, the dispersive behavior of the plasmon is projected out by the light polarization, so that most of the spectral weight of the non-linear kernel accumulates around the temperature-dependent $\omega_z(T)$, that corresponds to the plasma edge in the zero-momentum reflectivity. The resulting non-monotonic dependence of the kernel predicted for a driving frequency $\Omega < \omega_z(T = 0)$, as shown in Fig. 1d, closely resembles the results of Ref. [19] in single-layer LSCO superconductor. For what concerns instead bilayer YBCO the plasmon dispersion and the projection mechanism are crucial to account for the shift of the kernel resonance towards the high-energy plasmon $\omega_{z1} \approx 15$ THz, see Fig. 2d, while no signature remains at the lower plasmon $\omega_{z2} \approx 1.2$ THz measured by reflectivity, explaining the lack of any enhancement of the THG at the temperature where $\Omega = \omega_{z2}(T)$ in the measurements of Ref. [23], performed with $\Omega \sim 0.5$ THz. Conversely, the resonance condition $\Omega = \omega_{z1}(\bar{T})$ is achieved at a temperature \bar{T} so close to T_c that the resonance itself is washed out by the suppression of the stiffness, making the non-linear response kernel rather monotonous, as shown by the solid line in Fig. 2e. To make a quantitative comparison with the measurements of Ref. [23] we extracted the THG kernel $K(2\Omega, T)$ from the measured 3Ω component of the reflected field E_r . This can be achieved by implementing a modified Fresnel approach as[45]:

$$E_r \propto K(2\Omega) \left(\frac{2}{n(\Omega) + 1} \right)^3 \frac{1}{n(3\Omega) + n(\Omega)} \frac{1}{n(3\Omega) + 1} E_0^3, \quad (9)$$

where $n(\Omega)$ ($n(3\Omega)$) is the experimentally-measured index of refraction at Ω (3Ω). Eq. (9) is a modified Fresnel result which includes also the role played by the non-linear current[45]. As such, it differs slightly from the one presented in Ref. [23]. The resulting temperature dependence of the THG extracted from the experimental data of Ref. [23], shown as solid dots in Fig. 2(e), is in excellent agreement with our theoretical prediction, also shown as a solid line.

In summary, our work demonstrates how a two-plasmon excitation mechanism quantitatively explains the occurrence of enhanced non-linear response for pumping THz field polarized along the layer stacking direction in cuprate superconductors. The combined effect of the light polarization and the plasmon dispersion explains the existence of a resonant effect for pumping frequency matching the plasma edge in single-layer materials, while it accounts for a shift of the resonance frequency towards the larger out-of-plane plasma mode for bilayer structures. In the bilayer case a resonant effect could still be visible by pumping the system with a frequency slightly below the $\omega_{zT}(T = 0)$ or $\omega_{z1}(T = 0)$ value. However, the quasiparticle damping around ω_{zT} or ω_{z1} is consid-

erably larger than around ω_{z2} , as evidenced by the much weaker plasma edge at ω_{z1} in optics[34], leading presumably to a substantial broader resonance as compared to the single-layer case. On a more general perspective, the present results suggest the intriguing possibility to engineering artificial heterostructures of superconducting materials in order to tune the bilayer structure towards the desired resonance mode, eventually exploiting the Josephson-junction modulation induced by twisted structures[46]. At the same time, a full quantum description of the non-linear Josephson response, as the one provided in the present manuscript, provides the starting point for the understanding of the multidimensional spectrum obtained in two-dimensional THz protocols[47], in order to disentangle the intrinsic thermal effects from inhomogeneity broadening in unconventional cuprates.

Acknowledgements We acknowledge K. Katsumi for useful discussions and for providing us with the experimental data from Ref. [23]. We acknowledge financial support by Sapienza University under Ateneo projects RM12117A4A7FD11B and RP1221816662A977, and by European Community by ERC-SYN MORE-TEM G.A. No 951215.

* jacopo.fiore@uniroma1.it

† lara.benfatto@roma1.infn.it

- [1] X. C. Zhang, A. Shkurinov, and Y. Zhang, Extreme Terahertz science, *Nature Photonics* **11**, 16 (2017).
- [2] B. Green, S. Kovalev, V. Asgekar, G. Geloni, U. Lehnert, T. Golz, M. Kuntzsch, C. Bauer, J. Hauser, J. Voigtlaender, B. Wustmann, I. Koesterke, M. Schwarz, M. Freitag, A. Arnold, J. Teichert, M. Justus, W. Seidel, C. Ilgner, N. Awari, D. Nicoletti, S. Kaiser, Y. Laplace, S. Rajasekaran, L. Zhang, S. Winnerl, H. Schneider, G. Schay, I. Lorincz, A. A. Rauscher, I. Radu, S. Mährlein, T. H. Kim, J. S. Lee, T. Kampfrath, S. Wall, J. Heberle, A. Malnasi-Csizmadia, A. Steiger, A. S. Müller, M. Helm, U. Schramm, T. Cowan, P. Michel, A. Cavalleri, A. S. Fisher, N. Stojanovic, and M. Gensch, High-field high-repetition-rate sources for the coherent THz control of matter, *Scientific Reports* **6**, 22256 (2016).
- [3] S. Mährlein, A. Paarmann, M. Wolf, and T. Kampfrath, Terahertz sum-frequency excitation of a Raman-active phonon, *Physical Review Letters* **119**, 127402 (2017).
- [4] C. L. Johnson, B. E. Knighton, and J. A. Johnson, Distinguishing nonlinear Terahertz excitation pathways with two-dimensional spectroscopy, *Physical Review Letters* **122**, 073901 (2019).
- [5] M. Udina, T. Cea, and L. Benfatto, Theory of coherent-oscillations generation in Terahertz pump-probe spectroscopy: From phonons to electronic collective modes, *Physical Review B* **100**, 165131 (2019).
- [6] D. M. Juraschek and S. F. Mährlein, Sum-frequency ionic Raman scattering, *Physical Review B* **97**, 174302 (2018).
- [7] A. von Hoegen, R. Mankowsky, M. Fechner, M. Först, and A. Cavalleri, Probing the interatomic potential of

- solids with strong-field nonlinear phononics, *Nature* **555**, 79 (2018).
- [8] M. Först, C. Manzoni, S. Kaiser, Y. Tomioka, Y. Tokura, R. Merlin, and A. Cavalleri, Nonlinear phononics as an ultrafast route to lattice control, *Nature Physics* **7**, 854 (2011).
- [9] A. Subedi, A. Cavalleri, and A. Georges, Theory of nonlinear phononics for coherent light control of solids, *Physical Review B* **89**, 220301 (2014).
- [10] X. Li, T. Qiu, J. Zhang, E. Baldini, J. Lu, A. M. Rappe, and K. A. Nelson, Terahertz field-induced ferroelectricity in quantum paraelectric SrTiO₃, *Science* **364**, 1079 (2019).
- [11] F. Gabriele, M. Udina, and L. Benfatto, Non-linear Terahertz driving of plasma waves in layered cuprates, *Nature Communications* **12**, 752 (2021).
- [12] M. Basini, M. Udina, M. Pancaldi, V. Unikandanunni, S. Bonetti, and L. Benfatto, The ionic Kerr effect (2023), arxiv:2210.14053 [cond-mat].
- [13] A. S. Disa, T. F. Nova, and A. Cavalleri, Engineering crystal structures with light, *Nature Physics* **17**, 1087 (2021).
- [14] M. Kozina, M. Fechner, P. Marsik, T. van Driel, J. M. Glowina, C. Bernhard, M. Radovic, D. Zhu, S. Bonetti, U. Staub, and M. C. Hoffmann, Terahertz-driven phonon upconversion in SrTiO₃, *Nature Physics* **15**, 387 (2019).
- [15] Y. Laplace and A. Cavalleri, Josephson plasmonics in layered superconductors, *Advances in Physics: X* **1**, 387 (2016).
- [16] S. Rajasekaran, E. Casandru, Y. Laplace, D. Nicoletti, G. D. Gu, S. R. Clark, D. Jaksch, and A. Cavalleri, Parametric amplification of a superconducting plasma wave, *Nature Physics* **12**, 1012 (2016).
- [17] S. Rajasekaran, J. Okamoto, L. Mathey, M. Fechner, V. Thampy, G. D. Gu, and A. Cavalleri, Probing optically silent superfluid stripes in cuprates, *Science* **359**, 575 (2018).
- [18] K. A. Cremin, J. Zhang, C. C. Homes, G. D. Gu, Z. Sun, M. M. Fogler, A. J. Millis, D. N. Basov, and R. D. Averitt, Photoenhanced metastable c-axis electrodynamic in stripe-ordered cuprate La_{1.885}Ba_{0.115}CuO₄, *Proceedings of the National Academy of Sciences* **116**, 19875 (2019).
- [19] K. Kaj, K. A. Cremin, I. Hammock, J. Schalch, D. N. Basov, and R. D. Averitt, Terahertz third harmonic generation in c-axis La_{1.85}Sr_{0.15}CuO₄, *Physical Review B* **107**, L140504 (2023).
- [20] S. Zhang, Z. Sun, Q. Liu, Z. Wang, Q. Wu, L. Yue, S. Xu, T. Hu, R. Li, X. Zhou, J. Yuan, G. Gu, T. Dong, and N. Wang, Revealing the frequency-dependent oscillations in nonlinear Terahertz response induced by Josephson current, *National Science Review*, nwad163 (2023).
- [21] A. von Hoegen, M. Fechner, M. Först, N. Taherian, E. Rowe, A. Ribak, J. Porras, B. Keimer, M. Michael, E. Demler, and A. Cavalleri, Amplification of superconducting fluctuations in driven YBa₂Cu₃O_{6+x}, *Physical Review X* **12**, 031008 (2022).
- [22] D. Fu, D. Nicoletti, M. Fechner, M. Buzzi, G. D. Gu, and A. Cavalleri, Terahertz phase slips in striped La_{2-x}Ba_xCuO₄, *Physical Review B* **105**, L020502 (2022).
- [23] K. Katsumi, M. Nishida, S. Kaiser, S. Miyasaka, S. Tajima, and R. Shimano, Near-infrared light-induced superconducting-like state in underdoped YBa₂Cu₃O_y studied by c-axis Terahertz third-harmonic generation, *Physical Review B* **107**, 214506 (2023).
- [24] P. Coleman, *Introduction to Many-Body Physics* (Cambridge University Press, Cambridge, 2015).
- [25] N. Nagaosa, *Quantum Field Theory in Condensed Matter Physics* (Springer, Berlin, Heidelberg, 1999).
- [26] K. Tamasaku, Y. Nakamura, and S. Uchida, Charge dynamics across the CuO₂ planes in La_{2-x}Sr_xCuO₄, *Physical Review Letters* **69**, 1455 (1992).
- [27] C. C. Homes, T. Timusk, R. Liang, D. A. Bonn, and W. N. Hardy, Optical conductivity of c axis oriented YBa₂Cu₃O_{6.70}: Evidence for a pseudogap, *Physical Review Letters* **71**, 1645 (1993).
- [28] J. H. Kim, H. S. Somal, M. T. Czyzyk, D. van der Marel, A. Wittlin, A. M. Gerrits, V. H. M. Duijn, N. T. Hien, and A. A. Menovsky, Strong damping of the c-axis plasmon in high-T_c cuprate superconductors, *Physica C: Superconductivity* **247**, 297 (1995).
- [29] D. N. Basov, T. Timusk, B. Dabrowski, and J. D. Jorgensen, C-axis response of YBa₂Cu₄O₈: A pseudogap and possibility of Josephson coupling of CuO₂ planes, *Physical Review B* **50**, 3511 (1994).
- [30] D. van der Marel and A. Tsvetkov, Transverse optical plasmons in layered superconductors, *Czechoslovak Journal of Physics* **46**, 3165 (1996).
- [31] S. V. Dordevic, S. Komiya, Y. Ando, and D. N. Basov, Josephson plasmon and inhomogeneous superconducting state in La_{2-x}Sr_xCuO₄, *Physical Review Letters* **91**, 167401 (2003).
- [32] S. Savel'ev, V. A. Yampol'skii, A. L. Rakhmanov, and F. Nori, Terahertz Josephson plasma waves in layered superconductors: Spectrum, generation, nonlinear and quantum phenomena, *Reports on Progress in Physics* **73**, 026501 (2010).
- [33] S. Savel'ev, A. L. Rakhmanov, V. A. Yampol'skii, and F. Nori, Analogues of nonlinear optics using terahertz Josephson plasma waves in layered superconductors, *Nature Physics* **2**, 521 (2006).
- [34] W. Hu, S. Kaiser, D. Nicoletti, C. R. Hunt, I. Gierz, M. C. Hoffmann, M. Le Tacon, T. Loew, B. Keimer, and A. Cavalleri, Optically enhanced coherent transport in YBa₂Cu₃O_{6.5} by ultrafast redistribution of interlayer coupling, *Nature Materials* **13**, 705 (2014).
- [35] M. Hepting, L. Chaix, E. W. Huang, R. Fumagalli, Y. Y. Peng, B. Moritz, K. Kummer, N. B. Brookes, W. C. Lee, M. Hashimoto, T. Sarkar, J.-F. He, C. R. Rotundu, Y. S. Lee, R. L. Greene, L. Braicovich, G. Ghiringhelli, Z. X. Shen, T. P. Devereaux, and W. S. Lee, Three-dimensional collective charge excitations in electron-doped copper oxide superconductors, *Nature* **563**, 374 (2018).
- [36] J. Lin, J. Yuan, K. Jin, Z. Yin, G. Li, K.-J. Zhou, X. Lu, M. Dantz, T. Schmitt, H. Ding, H. Guo, M. P. M. Dean, and X. Liu, Doping evolution of the charge excitations and electron correlations in electron-doped superconducting La_{2-x}Ce_xCuO₄, *npj Quantum Materials* **5**, 1 (2020).
- [37] A. Nag, M. Zhu, M. Bejas, J. Li, H. C. Robarts, H. Yamase, A. N. Petsch, D. Song, H. Eisaki, A. C. Walters, M. García-Fernández, A. Greco, S. M. Hayden, and K.-J. Zhou, Detection of acoustic plasmons in hole-doped lanthanum and bismuth cuprate superconductors using resonant inelastic X-ray scattering, *Physical Review Letters* **125**, 257002 (2020).
- [38] L. Benfatto, A. Toschi, and S. Caprara, Low-energy phase-only action in a superconductor: A comparison

- with the XY model, *Physical Review B* **69**, 184510 (2004).
- [39] Z. Sun, M. M. Fogler, D. N. Basov, and A. J. Millis, Collective modes and terahertz near-field response of superconductors, *Physical Review Research* **2**, 023413 (2020).
- [40] See supplementary material.
- [41] F. Gabriele, C. Castellani, and L. Benfatto, Generalized plasma waves in layered superconductors: A unified approach, *Physical Review Research* **4**, 023112 (2022).
- [42] N. Sellati, F. Gabriele, C. Castellani, and L. Benfatto, Generalized Josephson plasmons in bilayer superconductors, *Physical Review B* **108**, 014503 (2023).
- [43] T. Cea, C. Castellani, and L. Benfatto, Nonlinear optical effects and third-harmonic generation in superconductors: Cooper pairs versus Higgs mode contribution, *Physical Review B* **93**, 180507 (2016).
- [44] F. Alpeggiani and L. C. Andreani, Josephson surface plasmons in spatially confined cuprate superconductors, *Physical Review B* **88**, 174513 (2013).
- [45] J. Fiore et al., in preparation.
- [46] S. Y. F. Zhao, N. Poccia, X. Cui, P. A. Volkov, H. Yoo, R. Engelke, Y. Ronen, R. Zhong, G. Gu, S. Plugge, T. Tummuru, M. Franz, J. H. Pixley, and P. Kim, Emergent Interfacial Superconductivity between Twisted Cuprate Superconductors (2021), arxiv:2108.13455 [cond-mat].
- [47] A. Liu, D. Pavicevic, M. H. Michael, A. G. Salvador, P. E. Dolgirev, M. Fechner, A. S. Disa, P. M. Lozano, Q. Li, G. D. Gu, E. Demler, and A. Cavalleri, Probing Inhomogeneous Cuprate Superconductivity by Terahertz Josephson Echo Spectroscopy (2023), arxiv:2308.14849 [cond-mat, physics:physics].